Origin of Diastereofacial Selectivity in Tertiary 2-Adamantyl Cations

Antonello Filippi,[†] Neil A. Trout,[‡] Patrick Brunelle,[§] William Adcock,[‡] Ted S. Sorensen,[§] and Maurizio Speranza*,[†]

Contribution from the Dipartimento di Studi di Chimica e Tecnologia delle Sostanze Biologicamente Attive, Università di Roma "La Sapienza", 00185 Roma, Italy, the Department of Chemistry, The Flinders University of South Australia, Adelaide, Australia 5001, and the Department of Chemistry, University of Calgary, Calgary, Alberta T2N 1N4, Canada

Received February 8, 2001

Abstract: The intrinsic factors governing the diastereofacial selectivity of 2-methyl-5-X-2-adamantyl cations (X = F ($\mathbf{I}_F$), Si(CH_3)$_3$ ($\mathbf{I}_{Si}$)) toward a representative nucleophile, i.e., methanol, have been investigated in the gas phase at 750 Torr and in the 20−80 °C temperature range. The kinetic results indicate that CH_3OH addition to $\mathbf{I}_F$ proceeds through tight transition structures (TS_F^{syn} and TS_F^{anti}) characterized by advanced C−O bonding. The same interactions are much less pronounced in the comparatively loose transition structures involved in the CH_3OH addition to $\mathbf{I}_{Si}$ (TS_{Si}^{syn} and TS_{Si}^{anti}). The experimental evidence indicates that the activation barriers for the anti addition to $\mathbf{I}_F$ and $\mathbf{I}_{Si}$ are invariably lower than those for the syn attack. Large adverse entropic factors account for the preferred syn diastereoselectivity observed in the reaction with $\mathbf{I}_F$. Entropy plays a minor role in the much looser transition structures involved in the reaction with $\mathbf{I}_{Si}$, which instead exhibits a preferred anti diastereoselectivity. Comparison of the above gas-phase results with related theoretical and solution data suggests that the diastereofacial selectivity of $\mathbf{I}_F$ and $\mathbf{I}_{Si}$ measured in solution arises in part from the differential solvation of the two faces of the pyramidalized ions.

Introduction

Understanding the origins of diastereofacial selectivity of a trigonal carbon center is crucial for predicting the outcome of important stereochemical syntheses.[1] Facial selectivity may be governed by several concurrent factors, such as steric hindrance, conformational effects, and chelation, as well as electronic factors. It is also highly sensitive to solvent and temperature effects. Disentanglement of electronic factors from the others is achieved by using rigid systems, such as the 2-methyl-5-X-2-adamantyl cation $\mathbf{I}_X$ Chart 1), where the X substituent is sufficiently remote from the trigonal center not to influence it either sterically or coordinatively. Depending upon the electronic properties of X, ions $\mathbf{I}_X$ display diametrically opposite stereochemistry. Syn (or *zu*) approach of the nucleophile is favored when X is a σ-electron-withdrawing substituent (e.g., in $\mathbf{I}_F$)). When instead X is a σ-electron-donating substituent, the nucleophile is preferentially directed to the anti (or *en*) face (e.g., in $\mathbf{I}_{Si}$)). This selectivity has been interpreted in terms of differential hyperconjugative stabilization of syn and anti transition structures (TS).[2−6] However, far from defined is the mode whereby hyperconjugative stabilization operates, whether through electrostatic or orbital interactions or both.[4]

Though entropy surely contributes to syn and anti TS free energies, its role in controlling stereodifferentiation is rarely appreciated.[7] Yet, the idea that entropy may govern the stereoselectivity of the nucleophilic attack on $\mathbf{I}_X$ cannot be dismissed a priori. This paper is aimed at evaluating the contribution of entropic factors on the diastereoselectivity of the nucleophilic attack of CH_3OH on two representative 2-methyl-5-X-adamantyl cations, i.e., $\mathbf{I}_F$ and $\mathbf{I}_{Si}$. The reaction takes place in an inert gaseous medium (either CH_4 or CH_3F at 750 Torr) to minimize any environmental effects on diastereoselectivity. The relatively high pressures used ensure the complete thermalization of all the active species involved.

Chart 1

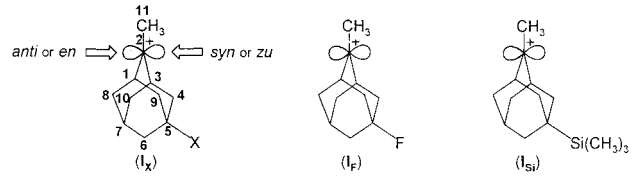

Methodology. Tertiary cations $\mathbf{I}_F$ and $\mathbf{I}_{Si}$ are generated in the gas phase by two different procedures. Procedure A involves the protonation of the corresponding 2-methylene-5-X-adamantane $\mathbf{1}_X$ by the $C_nH_5^+$ (n = 1, 2) Brönsted acids, formed from γ-irradiation (^{60}Co γ-rays, T = 20−80 °C) of gaseous CH_4 mixtures. Protonation takes place in the presence of traces of a nucleophile ($CH_3{}^{18}OH$, ^{18}O-content, 95%), a radical scavenger (O_2), and a powerful base B ((C_2H_5)$_3$N) (path i of Scheme 1).[8] In procedure B, CH_3F is used as the bulk gas, instead of CH_4, and $H_2{}^{18}O$ (^{18}O-content, >97%) as the nucleophile, instead of $CH_3{}^{18}OH$. Irradiation of the $CH_3F/H_2{}^{18}O$ gives rise to the formation of $CH_3{}^{18}OH_2^+$ ions in the complete absence of neutral $CH_3{}^{18}OH$ molecules (Scheme 2 (Y = F)).[9] Under such conditions, the ^{18}O-labeled ethereal products $\mathbf{2}^Z_X$ and $\mathbf{2}^E_X$ must

[†] University of Roma "La Sapienza".
[‡] The Flinders University of South Australia.
[§] University of Calgary.

(1) For reviews on this topic, see the special issue: *Chem. Rev.* **1999**, *99* (5).
(2) Cheung, C. K.; Tseng, L. T.; Lin, M. H.; Srivastava, S.; le Noble, W. J. *J. Am. Chem. Soc.* **1986**, *108*, 1598; **1987**, *109*, 7239.
(3) Srivastava, S.; le Noble, W. J. *J. Am. Chem. Soc.* **1987**, *109*, 5874.
(4) Adcock, W.; Cotton, J.; Trout, N. A. *J. Org. Chem.* **1994**, *59*, 1867.
(5) Herrmann, R.; Kirmse, W. *Liebigs Ann.* **1995**, 699.
(6) Adcock, W.; Head, N. J.; Lokan, N. R.; Trout, N. A. *J. Org. Chem.* **1997**, *62*, 6177.
(7) Rosenberg, R. E.; Vilardo, J. S. *Tetrahedron Lett.* **1996**, *37*, 2185.
(8) Lias, S. G.; Hunter, E. P. L. *J. Phys. Chem. Ref. Data* **1998**, *27*, 413.

10.1021/ja010352l CCC: $20.00
Published on Web 06/08/2001

Scheme 1

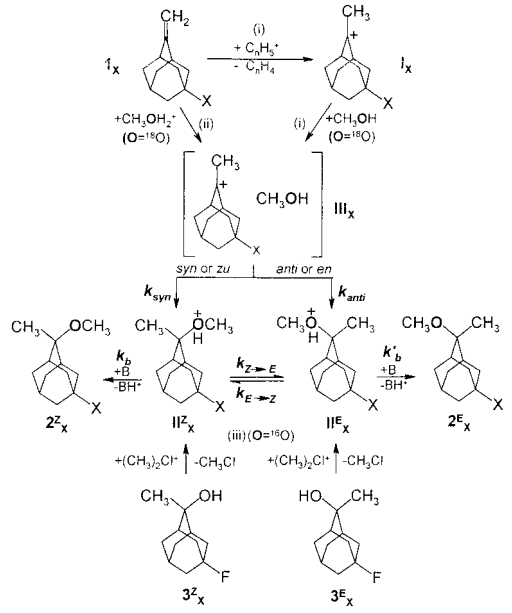

necessarily arise from the *intracomplex* addition between the two moieties of adduct $\mathbf{III}_X$, generated by proton transfer in the encounter between olefin $\mathbf{1}_X$ and $CH_3{}^{18}OH_2{}^+$ (path ii of Scheme 1).

A set of experiments has been carried out to evaluate the extent of $\mathbf{II}^E_X \rightleftarrows \mathbf{II}^Z_X$ epimerization ($k_{E\rightarrow Z}$ vs $k_{Z\rightarrow E}$ in Scheme 1) prior to neutralization (k_b and k'_b in Scheme 1). The gaseous samples used for this purpose were identical to those used in procedure B with the only important difference being that CH_3Cl (750 Torr), and not CH_3F, was employed as the bulk component. This prevents the radiolytic formation of $CH_3{}^{18}OH_2{}^+$ ions to any significant extent. In fact, contrary to $(CH_3)_2F^+$, the $(CH_3)_2Cl^+$ ions react very slowly with the water molecules present in the mixture (Scheme 2; Y = Cl).[10] As a consequence, the oxonium intermediates $\mathbf{II}^E_X$ and $\mathbf{II}^Z_X$ are directly formed from $(CH_3)_2Cl^+$-methylation of the corresponding alcohol, i.e., (*E*)- and (*Z*)-2-methyl-5-X-2-hydroxyadamantane ($\mathbf{3}^E_X$ and $\mathbf{3}^Z_X$, respectively; X = F or $Si(CH_3)_3$), and any contribution from other conceivable pathways, involving $CH_3{}^{18}OH_2{}^+$, is excluded (route (iii) of Scheme 1).[11]

Experimental Section

Materials. Methane, methyl fluoride, and oxygen were high-purity gases from UCAR Specialty Gases N. V. and were used without further purification. $H_2{}^{18}O$ (^{18}O-content, >97%), $CH_3{}^{18}OH$ (^{18}O-content, 95%), and $(C_2H_5)_3N$ were purchased from ICON Services and Aldrich Co., respectively. 2-Methylene-5-fluoroadamantane ($\mathbf{1}_F$), 2-methylene-5-(trimethylsilyl)adamantane ($\mathbf{1}_{Si}$), the *E*/*Z* mixture of the 2-methyl-5-fluoro-2-hydroxyadamantanes ($\mathbf{3}^E_F/\mathbf{3}^Z_F$), and the *E*/*Z* mixture of the 2-methyl-5-trimethylsilyl-2-hydroxyadamantanes ($\mathbf{3}^E_{Si}/\mathbf{3}^Z_{Si}$), used as starting substrates, were prepared according to previously described procedures.[2,4] The $\mathbf{3}^E_F/\mathbf{3}^Z_F$ mixture (*E*/*Z* = 66/34) was separated by preparative GLC on a 10% Silicone OV17 on Chromosorb Wax 80−100 mesh, 2-m-long, 4.5-mm-i.d., stainless steel column, operated at $50 < T < 100$ °C, 10 °C min^{-1}. The melting points and ^{13}C NMR data of the *E*- and *Z*-tertiary fluoroalcohols were in accord with those reported in the literature.[2,4] The $\mathbf{3}^E_{Si}/\mathbf{3}^Z_{Si}$ mixture (130 mg, *Z*/*E* = 51/49) was separated by column chromatography (silica, 5% EtOAc/hexane as eluent) to afford the pure epimers as white solids. *E*-Isomer ($\mathbf{3}^E_{Si}$) (50 mg, R_f = 0.19, 5% EtOAc/hexane); mp 88−90 °C; ^{13}C NMR ($CDCl_3$, relative to Me_4Si) δ 38.56 (C1,3), 73.79 (C2), 34.96 (C4,9), 20.33 (C5), 37.62 (C6), 26.50 (C7), 32.88 (C8,10), 27.19 (Me). *Z*-Isomer ($\mathbf{3}^Z_{Si}$) (35 mg, R_f = 0.26, 5% EtOAc/hexane); mp 86−87 °C; ^{13}C NMR ($CDCl_3$, relative to Me_4Si) δ 38.56 (C1,3), 73.58 (C2), 32.48 (C4,9), 19.72 (C5), 37.62 (C6), 26.95 (C7), 35.01 (C8,10), 27.49 (Me). The spectra were assigned by additivity methodology.[12] *E*-Isomer ($\mathbf{3}^E_{Si}$) (calcd): 38.59 (C1,3), 73.89 (C2), 34.57 (C4,9), 20.25 (C5), 37.75 (C6), 26.51 (C7), 33.00 (C8,10). *Z*-Isomer ($\mathbf{3}^Z_{Si}$) (calcd): δ 38.59 (C1,3), 73.89 (C2), 32.41 (C4,9), 19.74 (C5), 37.75 (C6), 27.02 (C7), 35.16 (C8,10).

2-Methyl-2-methoxyadamantane. To a solution of 2-chloro-2-methyladamantane (100 mg, 0.54 mmol) in dry methanol (14 mL) was added silver nitrate (192 mg) under N_2. The reaction was monitored by GLC until complete. The solution was filtered, followed by evaporation and passage through a short silica column eluting with 10% Et_2O/hexane, and afforded the ether as a colorless oil (50 mg, 51%). ^{13}C NMR ($CDCl_3$, relative to Me_4Si) δ 35.79 (C1,3), 77.32 (C2), 32.60 (C4,9), 26.93 (C5), 38.27 (C6), 27.72 (C7), 34.67 (C8,10), 47.29 (OMe), 20.49 (Me); ^1H NMR ($CDCl_3$, relative to $CHCl_3$) δ 3.19 (s, 3H), 2.12 (d, 2H), 1.83−1.40 (m, 12H), 1.24 (s, 3H); MS *m*/*z* (M^+) calcd for $C_{12}H_{20}O$ 180.15141, found 180.1513.

(*E*)-2-Methyl-5-(trimethylsilyl)-2-methoxyadamantane ($\mathbf{2}^E_{Si}$). To a slurry of prewashed 50% NaH (10 mg) in THF (1 mL) under N_2 was added a solution of alcohol $\mathbf{3}^E_{Si}$ (10 mg, 42 μmol) in THF (1 mL), and the resultant mixture was allowed to stir for 30 min at room temperature, before dropwise addition of MeI (200 μL). The solution was brought to reflux for 10 min before cooling and allowed to stir overnight. The usual workup afforded the title compound as a colorless oil after chromatography (silica, 5% EtOAc/hexane, R_f = 0.56) (7 mg, 66%). ^{13}C NMR ($CDCl_3$, relative to Me_4Si) δ 35.35 (C1,3), 77.26 (C2), 34.56 (C4,9), 20.57 (C5), 37.72 (C6), 26.51 (C7), 32.62 (C8,10), 47.27 (OMe), 20.44 (Me), −5.46 ($SiMe_3$); ^1H NMR ($CDCl_3$, relative to $CHCl_3$) δ 3.19 (s, 3H), 2.15 (d, 2H), 1.80−1.40 (m, 13H), 1.21 (s, 3H), −0.10 (s, 9H). The spectrum was assigned by additivity methodology.[12] *E*-somer ($\mathbf{2}^E_{Si}$) (calcd): 35.26 (C1,3), 77.34 (C2), 34.10 (C4,9), 20.43 (C5), 37.70 (C6), 26.40 (C7), 32.62 (C8,10). MS *m*/*z* (M^+) calcd for $C_{15}H_{28}OSi$ 252.19094, found 252.2050.

(*E*/*Z*)-2-Methyl-5-(trimethylsilyl)-2-methoxyadamantane ($\mathbf{2}^E_{Si}/\mathbf{2}^Z_{Si}$). The tertiary chloride mixture obtained from the hydrochlorination of 2-methylene-5-trimethylsilyladamantane ($\mathbf{1}_{Si}$) (*E*/*Z* = 65/35) was treated with silver nitrate in methanol to provide the title ethers (*E*/*Z* = 53/47) as previously described for 2-methoxy-2-methyladamantane. *E*-Isomer ($\mathbf{2}^E_{Si}$): ^{13}C NMR ($CDCl_3$, relative to Me_4Si) δ 35.35 (C1,3), 77.26 (C2), 34.69 (C4,9), 20.59 (C5), 37.74 (C6), 26.54 (C7), 32.64 (C8,10), 47.26 (OMe), 20.44 (Me), −5.45 ($SiMe_3$). *Z*-Isomer ($\mathbf{2}^Z_{Si}$); 35.38 (C1,3), 77.26 (C2), 32.64 (C4,9), 19.58 (C5), 37.67 (C6), 27.28 (C7), 34.59 (C8,10), 47.34 (OMe), 20.65 (Me), −5.45 ($SiMe_3$). The spectra were assigned by additivity methodology.[12] *E*-Isomer ($\mathbf{2}^E_{Si}$) (calcd): 35.26 (C1,3), 77.34 (C2), 34.10 (C4,9), 20.43 (C5), 37.70 (C6), 26.40 (C7), 32.62 (C8,10). *Z*-Isomer ($\mathbf{2}^Z_{Si}$) (calcd): 35.26 (C1,3), 77.34 (C2), 32.03 (C4,9), 19.63 (C5), 37.70 (C6), 27.19 (C7), 34.69 (C8,10).

(E/Z)-2-Methyl-5-fluoro-2-methoxyadamantane ($\mathbf{2}^E_F/\mathbf{2}^Z_F$). The ($\mathbf{2}^E_F/\mathbf{2}^Z_F$) mixture (100 mg, 70%) (*E*/*Z* = 67/33) was obtained using the NaH/MeI method as described above. ^{13}C NMR ($CDCl_3$, relative to Me_4Si) δ *E*-isomer ($\mathbf{2}^E_F$), 38.51, J_{CF} = 10.38 Hz (C1,3), 76.02 J_{CF} = 1.22 Hz (C2), 39.19 J_{CF} = 18.31 Hz (C4,9), 92.45 J_{CF} = 183.72 Hz (C5), 43.31 J_{CF} = 16.48 Hz (C6), 29.90 J_{CF} = 9.77 Hz (C7), 31.03 J_{CF} = 2.44 Hz (C8,10), 47.98 (OMe), 20.58 (Me). *Z*-Isomer ($\mathbf{2}^Z_F$), 38.84 J_{CF} = 10.38 Hz (C1,3), 75.63 J_{CF} = 2.44 Hz (C2), 37.58 J_{CF} = 18.31 Hz (C4,9), 91.79 J_{CF} = 183.11 Hz (C5), 43.23 J_{CF} = 17.09 Hz (C6), 30.70 J_{CF} = 9.77 Hz (C7), 33.01 J_{CF} = 1.83 Hz (C8,10), 47.42 (OMe), 19.52 J_{CF} = 2.44 Hz (Me). The spectra were assigned by the additivity of substituent effects on chemical shifts of the adamantane ring[12] as well as the relative intensity of the peaks (*E*/*Z* = 67/33) and the

(9) Blint, R. J.; McMahon, T. B.; Beauchamp, J. L. *J. Am. Chem. Soc.* **1974**, *96*, 1269.

(10) Speranza, M.; Troiani, A. *J. Org. Chem.* **1998**, *63*, 1020.

(11) A direct proof of the inertness of $(CH_3)_2Cl^+$ ions toward water arises from the observation that the ethereal products, recovered in the $CH_3Cl/H_2{}^{18}O/\mathbf{1}_X$ mixtures, contain less than 3% of the ^{18}O label.

(12) Srivastava, S.; Cheung, C. K.; le Noble, W. J. *Magn. Reson. Chem.* **1985**, *23*, 232.

Scheme 2

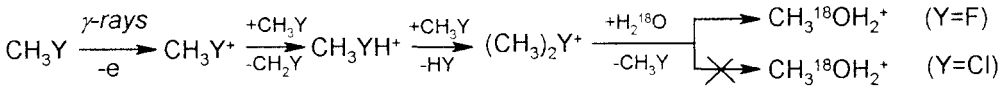

characteristic carbon−fluorine coupling constant pattern in 1-fluoroadamantanes.[13] *E*-Isomer ($\mathbf{2}^{E}_{F}$) (calcd): 38.89 (C1,3), 75.46 (C2), 39.69 (C4,9), 91.73 (C5), 43.29 (C6), 30.03 (C7), 30.74 (C8,10). *Z*-Isomer ($\mathbf{2}^{Z}_{F}$) (calcd): 38.89 (C1,3), 75.46 (C2), 37.62 (C4,9), 90.94 (C5), 43.29 (C6), 30.82 (C7), 32.81 (C8,10). MS *m*/*z* (M^+) calcd for $C_{12}H_{19}O$ 198.14198, found 198.1428.

Procedure. The gaseous mixtures were prepared by conventional procedures with the use of a greaseless vacuum line. The starting adamantane substrate, the labeled nucleophile (either $H_2{}^{18}O$ (^{18}O-content, >97%) or $CH_3{}^{18}OH$ (^{18}O-content, 95%)), the thermal radical scavenger O_2, and the base B = $(C_2H_5)_3N$ were introduced into carefully outgassed 130-mL Pyrex bulbs, each equipped with a break-seal tip. The bulbs were filled with the bulk gas (CH_3Y; Y = H, F, Cl (750 Torr)), cooled to the liquid nitrogen temperature, and sealed off. The gaseous mixtures were submitted to irradiation at a constant temperature ranging from 20 to 140 °C in a ^{60}Co source (dose, 2×10^4 Gy; dose rate, 1×10^4 Gy h^{-1}, determined with a neopentane dosimeter). Control experiments, carried out at doses ranging from 1×10^4 to 1×10^5 Gy, showed that the relative yields of products are largely independent of the dose. The radiolytic products were analyzed by GLC on a MEGADEX DACTBS-β (30% 2,3-di-*O*-acetyl-6-*O*-(*tert*-butyldimethylsilyl)-β-cyclodextrin in OV 1701; 25-m-long, 0.25-mm-i.d. d_f, 0.25 μm) fused-silica column, at $60 < T < 170$ °C, 5 °C min^{-1}. The products were identified by comparison of their retention volumes with those of authentic standard compounds and their identity confirmed by GLC−MS. Their yields were determined from the areas of the corresponding eluted peaks, using benzyl alcohol as the internal standard and individual calibration factors to correct for the detector response. Blank experiments were carried out to exclude the occurrence of thermal decomposition and isomerization of the starting substrates as well as the epimerization of their ethereal products within the temperature range investigated.

The extent of ^{18}O incorporation into the radiolytic products was determined by GLC−MS, setting the mass analyzer in the selected ion mode (SIM). The ion fragments at *m*/*z* = 183 (^{16}O-$[M - CH_3]^+$) and *m*/*z* = 185 (^{18}O-$[M - CH_3]^+$) were monitored to analyze the epimeric $\mathbf{2}^{E}_{F}$ and $\mathbf{2}^{Z}_{F}$ ethers. The ion fragments at *m*/*z* = 237 (^{16}O-$[M - CH_3]^+$) and *m*/*z* = 239 (^{18}O-$[M - CH_3]^+$) were examined to analyze the epimeric $\mathbf{2}^{E}_{Si}$ and $\mathbf{2}^{Z}_{Si}$ ethers.

Computational Details. Quantum chemical calculations were performed on PC-based computers and the Linux operating system, using the A7 version of the suite of programs in Gaussian 98.[14] The 6-31G* basis set was employed using the B3LYP hybrid density functional procedure.[15] At the same level of theory, frequency calculations were performed for all the optimized structures to ascertain their minimum or transition-state nature. Thermal contribution to enthalpy at 298 K and 1 atm, which includes the effects of translation, rotation, and vibration, was evaluated by classical statistical thermodynamics within the approximation of ideal gas, rigid rotor, and harmonic oscillator behavior and using the recommended scale factor (0.98) for frequencies and zero point energy correction.[16]

Results

Theoretical Calculations. A global minimum structure (stationary point, all real frequencies) has been identified on the $\mathbf{I}_F$ surface at the B3LYP/6-31G* level of theory, whose structure is schematized in Figure 1a. Accordingly, $\mathbf{I}_F$ displays a distorted structure with a C11−H hydrogen coplanar to the C5−F bond and oriented toward it. The C1−C2−C3 bridge leans away from the F substituent by $\theta = 14.6°$ using the angle definitions shown in Figure 1. In addition, the C2−C11 bond leans away from the F substituent by $\varphi = 6.2°$ relative to the C1−C2−C3 plane. A global minimum structure has been identified also on the $\mathbf{I}_{Si}$ B3LYP/6-31G* surface. Its geometry is illustrated in Figure 1b. It presents a C11−H hydrogen coplanar to the C5−$Si(CH_3)_3$ bond, but oriented away from it. The C1−C2−C3 bridge leans toward the $Si(CH_3)_3$ substituent by $\theta = 12.7°$ as defined in Figure 1. The C2−C11 bond leans further toward the $Si(CH_3)_3$ substituent by $\varphi = 8.1°$ relative to the C1−C2−C3 plane.

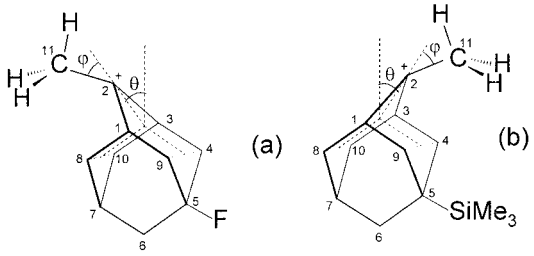

Figure 1. B3LYP/6-31G*-optimized geometries of 2-methyl-5-fluoro-2-adamantyl cation $\mathbf{I}_F$ (a) and 2-methyl-5-(trimethylsilyl)-2-adamantyl cation $\mathbf{I}_{Si}$ (b). Bond distances in structure a: C1−C8 = C3−C10 = 1.611 Å; C1−C9 = C3−C4 = 1.546 Å. Bond distances in structure b: C1−C8 = C3−C10 = 1.551 Å; C1−C9 = C3−C4 = 1.632 Å. Angle θ is defined as the deviation of the C1−C2−C3 plane from the bisector of the 8−10, 1−3, 9−4 midpoint lines. Angle φ is defined as the C2−C11 bond deviation from the C1−C2−C3 plane in each case.

Table 1. B3LYP/6-31G* Reaction Enthalpies

reaction	ΔH_{298} (kcal mol^{-1})
$\mathbf{II}^{E}_{F} \rightarrow \mathbf{II}^{Z}_{F}$	−0.81
$\mathbf{II}^{E}_{Si} \rightarrow \mathbf{II}^{Z}_{Si}$	+0.03
$\mathbf{II}^{E}_{F} \rightarrow \mathbf{I}_F + CH_3OH$	+12.93
$\mathbf{II}^{Z}_{F} \rightarrow \mathbf{I}_F + CH_3OH$	+13.74
$\mathbf{II}^{E}_{Si} \rightarrow \mathbf{I}_{Si} + CH_3OH$	+7.39
$\mathbf{II}^{Z}_{Si} \rightarrow \mathbf{I}_{Si} + CH_3OH$	+7.37

The 298 K C−O bond enthalpies of $\mathbf{II}^{Z}_{X}$ and $\mathbf{II}^{E}_{X}$ and the 298 K $\mathbf{II}^{Z}_{X} \rightleftarrows \mathbf{II}^{E}_{X}$ epimerization enthalpies, calculated at the B3LYP/6-31G* level of theory, are listed in Table 1.

Radiolytic Experiments. Tables 2 and 3 report the absolute and relative yields of the ^{18}O-labeled ethers $\mathbf{2}^{E}_{X}$ and $\mathbf{2}^{Z}_{X}$ (X = F or $Si(CH_3)_3$, respectively) obtained from the *extra* (i) and *intracomplex* (ii) pathways of Scheme 1. The tables report average values obtained from several separate irradiations carried out under the same experimental conditions and whose reproducibility is expressed by the uncertainty level quoted. The ionic origin of ethers $\mathbf{2}^{E}_{X}$ and $\mathbf{2}^{Z}_{X}$ is demonstrated by the sharp decrease (over 80%) of their abundance as the $(C_2H_5)_3N$ concentration is quintupled.

The relative distribution of labeled ethers $\mathbf{2}^{Z}_{X}$ and $\mathbf{2}^{E}_{X}$ can be taken as representative of that of the corresponding ionic precursors $\mathbf{II}^{Z}_{X}$ and $\mathbf{II}^{E}_{X}$, if the efficiency of their neutralization by the strong base B = $(C_2H_5)_3N$ (proton affinity (PA) = 234.7

(13) Adcock, W.; Trout, N. A. *Magn. Reson. Chem.* **1998**, *36*, 181.

(14) Frish, M. J.; Trucks, G. W.; Schlegel, H. B.; Gill, P. M. W.; Johnson, B. G.; Robb, M. A.; Cheeseman, J. R.; Keith, T. A.; Petersson, G. A.; Montgomery, J. A.; Raghavachari, K.; Al-Laham, M. A.; Zakrzewski, V. G.; Ortiz, J. V.; Foresman, J. B.; Cioslowski, J.; Stefanov, B. B.; Nanayakkara, A.; Challacombe, M.; Peng, C. Y.; Ayala, P. Y.; Chen, W.; Wong, M. W.; Andres, J. L.; Repogle, E. S.; Gomperts, R.; Martin, R. L.; Fox, D. J.; Binkley, J. S.; Defrees, D. J.; Baker, J.; Stewart, J. P.; Head-Gordon, M.; Gonzales, C.; Pople, J. A. *Gaussian 98, Revision C. 2*, Gaussian, Inc., Pittsburgh, PA, 1995.

(15) (a) Becke, A. D. *J. Chem. Phys.* **1993**, *98*, 1372, 5648. (b) Lee, C.; Yang, W.; Parr, R. G. *Phys. Rev. B* **1988**, *37*, 785.

(16) Scott, A. P.; Radom, L. *J. Phys. Chem.* **1996**, *100*, 16502.

Table 2. ^{18}O-Labeled Product Distribution from the Gas-Phase Attack of Gaseous Acids on $\mathbf{1}_F$ in the Presence of B═N(CH$_3$)$_3$[a]

rxn path	R^{18}OH (Torr)	B (Torr)	T (°C)	τ[b] ($\times 10^8$ s)	[$\mathbf{2}^{Z}_F$]	[$\mathbf{2}^{E}_F$][c]	absolute yield[d] ($G_{(M)} \times 10^2$)
i	CH$_3$, 1.33	0.39	20	6.78	0.614	0.386	10.7
i	CH$_3$, 1.32	0.44	40	6.45	0.644	0.356	8.9
i	CH$_3$, 1.33	0.44	60	6.88	0.656	0.344	9.2
i	CH$_3$, 1.23	0.44	80	7.32	0.650	0.350	9.7
ii	H, 3.11	0.39	20	6.78	0.733	0.267	0.4
ii	H, 2.89	0.44	40	6.45	0.725	0.275	1.2
ii	H, 2.90	0.44	60	6.88	0.727	0.273	0.7
ii	H, 3.06	0.44	80	7.32	0.717	0.283	0.2

[a] Bulk gas, 750 Torr; $\mathbf{1}_F$, 0.2−0.3 Torr; O_2, 4 Torr; radiation dose, 2×10^4 Gy (dose rate, 1×10^4 Gy h^{-1}). [b] Reaction time, τ, calculated from the reciprocal of the first-order collision constant between intermediates $\mathbf{II}^{E}_F$ and $\mathbf{II}^{Z}_F$ and B. [c] Each value is the average of several determinations, with an uncertainty level of ∼10%. [d] $G_{(M)}$ as the number of molecules M produced per 100 eV of absorbed energy.

Table 3. ^{18}O-Labeled Product Distribution from the Gas-Phase Attack of Gaseous Acids on $\mathbf{1}_{Si}$ in the Presence of B═N(CH$_3$)$_3$[a]

rxn path	R^{18}OH (Torr)	B (Torr)	T (°C)	τ[b] ($\times 10^8$ s)	[$\mathbf{2}^{Z}_{Si}$]	[$\mathbf{2}^{E}_{Si}$][c]	absolute yield[d] ($G_{(M)} \times 10^2$)
i	CH$_3$, 0.88	0.48	20	5.72	0.409	0.591	0.6
i	CH$_3$, 0.85	0.46	40	6.40	0.445	0.555	1.0
i	CH$_3$, 0.77	0.47	60	6.68	0.432	0.568	0.7
i	CH$_3$, 1.00	0.53	80	6.30	0.480	0.520	0.8
ii	H, 3.05	0.51	20	5.38	0.363	0.637	1.4
ii	H, 3.29	0.50	40	5.88	0.385	0.615	1.2
ii	H, 3.08	0.50	60	6.28	0.469	0.531	0.7
ii	H, 3.26	0.50	80	6.68	0.508	0.492	0.4

[b] Bulk gas, 750 Torr; $\mathbf{1}_{Si}$, 0.2−0.3 Torr; O_2, 4 Torr; radiation dose, 2×10^4 Gy (dose rate, 1×10^4 Gy h^{-1}). [b] Reaction time, τ, calculated from the reciprocal of the first-order collision constant between intermediates $\mathbf{II}^{E}_{Si}$ and $\mathbf{II}^{Z}_{Si}$ and B. [c] Each value is the average of several determinations, with an uncertainty level of ∼10%. [d] $G_{(M)}$ as the number of molecules M produced per 100 eV of absorbed energy.

kcal mol^{-1})[8] is taken equal to unity. In this frame, the rate constant ratio k_{syn}/k_{anti} of Scheme 1 can be expressed by the [$\mathbf{2}^{Z}_X$]/[$\mathbf{2}^{E}_X$] ratio, once corrected by the extent of $\mathbf{II}^{Z}_X \rightleftarrows \mathbf{II}^{E}_X$ epimerization by the time τ of their neutralization with the strong base B ($\tau = (k_b[B])^{-1}$) at each temperature.[17]

This piece of information is obtained by generating directly the $\mathbf{II}^{Z}_X$ and $\mathbf{II}^{E}_X$ intermediates by route iii of Scheme 1 and by measuring their epimerization rates ($k_{E\rightarrow Z}$ vs $k_{Z\rightarrow E}$) under conditions similar to those of Tables 2 and 3. The yield factors of the unlabeled ethers $\mathbf{2}^{Z}_X$ and $\mathbf{2}^{E}_X$, obtained from attack of $(CH_3)_2Cl^+$ ions on either $\mathbf{3}^{Z}_X$ or $\mathbf{3}^{E}_X$ in the presence of the base B = $(C_2H_5)_3N$, are given in Tables 4 (X = F) and 5 (X = Si(CH$_3$)$_3$) under the ζ and ϵ headings, respectively.

Taking into account that, during its lifetime τ, $\mathbf{II}^{E}_X$ epimerizes by the ζ fraction (and $\mathbf{II}^{Z}_X$ by the ϵ fraction), the $k_{Z\rightarrow E}$ and $k_{E\rightarrow Z}$ rate constants can be expressed as follows:

$$k_{Z\rightarrow E} = \frac{\epsilon_{eq}}{\tau} \ln\left\{\frac{\epsilon_{eq}}{\epsilon_{eq} - \epsilon}\right\} \quad \text{with} \quad \epsilon_{eq} = \frac{K_{eq}}{1 + K_{eq}}$$

(eqs VII and X of Appendix)

and

$$k_{E\rightarrow Z} = \frac{\zeta_{eq}}{\tau} \ln\left\{\frac{\zeta_{eq}}{\zeta_{eq} - \zeta}\right\} \quad \text{with} \quad \zeta_{eq} = \frac{1}{1 + K_{eq}}$$

(eqs VIII and XI of Appendix)

The $\mathbf{II}^{Z}_X \rightleftarrows \mathbf{II}^{E}_X$ equilibrium constant K_{eq} can be calculated from the ratio between the ζ term from $\mathbf{II}^{E}_X$ and the ϵ term from $\mathbf{II}^{Z}_X$, measured under the same experimental conditions.

$$K_{eq} = \epsilon/\zeta \quad \text{(eq XVII of Appendix)}$$

Table 4. Kinetics of Gas-Phase Epimerization of $\mathbf{II}^{E}_F$ and $\mathbf{II}^{Z}_F$ in the Presence of B═N(CH$_3$)$_3$[a]

substrate	B (Torr)	T (°C)	τ[b] ($\times 10^8$ s)	ζ[c]	$k_{E\rightarrow Z}$[d] ($\times 10^{-6}$ s^{-1})	K_{eq}[d]
$\mathbf{3}^{E}_F$ (0.24)	0.72	40	3.93	0.038	1.00 (6.00)	0.92 (−0.04)
$\mathbf{3}^{E}_F$ (0.19)	0.68	50	4.30	0.052	1.27 (6.10)	0.81 (−0.09)
$\mathbf{3}^{E}_F$ (0.28)	0.85	60	3.56	0.061	1.81 (6.26)	0.90 (−0.05)
$\mathbf{3}^{E}_F$ (0.29)	0.81	80	3.97	0.097	2.68 (6.43)	0.76 (−0.12)
$\mathbf{3}^{E}_F$ (0.25)	0.90	90	3.68	0.126	3.91 (6.59)	0.87 (−0.06)
$\mathbf{3}^{E}_F$ (0.22)	0.80	100	4.26	0.213	6.16 (6.79)	0.65 (−0.19)
$\mathbf{3}^{E}_F$ (0.23)	0.74	120	4.86	0.325	9.52 (6.98)	0.63 (−0.20)

substrate	B (Torr)	T (°C)	τ[b] ($\times 10^8$ s)	ϵ[c]	$k_{Z\rightarrow E}$[d] ($\times 10^{-6}$ s^{-1})	K_{eq}[d]
$\mathbf{3}^{Z}_F$ (0.20)	0.72	40	3.93	0.035	0.92 (5.96)	0.92 (−0.04)
$\mathbf{3}^{Z}_F$ (0.32)	0.68	50	4.30	0.042	1.02 (6.01)	0.81 (−0.09)
$\mathbf{3}^{Z}_F$ (0.23)	0.85	60	3.56	0.055	1.64 (6.22)	0.90 (−0.04)
$\mathbf{3}^{Z}_F$ (0.22)	0.81	80	3.97	0.074	2.04 (6.31)	0.76 (−0.12)
$\mathbf{3}^{Z}_F$ (0.27)	0.90	90	3.68	0.110	3.41 (6.53)	0.87 (−0.06)
$\mathbf{3}^{Z}_F$ (0.20)	0.80	100	4.26	0.138	3.99 (6.60)	0.65 (−0.19)
$\mathbf{3}^{Z}_F$ (0.27)	0.74	120	4.86	0.205	6.00 (6.78)	0.63 (−0.20)

[a] CH_3Cl, 750 Torr; $H_2{}^{18}O$, 3 Torr; O_2, 6 Torr; radiation dose, 2×10^4 Gy (dose rate, 1×10^4 Gy h^{-1}). [b] Reaction time, τ, calculated from the reciprocal of the first-order collision constant between intermediates $\mathbf{II}^{E}_F$ and $\mathbf{II}^{Z}_F$ and B. [c] $\zeta = [\mathbf{2}^{Z}_F]/([\mathbf{2}^{E}_F] + [\mathbf{2}^{Z}_F])$; $\epsilon = [\mathbf{2}^{E}_F]/([\mathbf{2}^{E}_F] + [\mathbf{2}^{Z}_F])$. Each value is the average of several determinations, with an uncertainty level of ∼5%. [d] See text; log k and log K_{eq} in parentheses.

Table 5. Kinetics of Gas-Phase Epimerization of $\mathbf{II}^{E}_{Si}$ and $\mathbf{II}^{Z}_{Si}$ in the Presence of B═N(CH$_3$)$_3$[a]

substrate	B (Torr)	T (°C)	τ[b] ($\times 10^8$ s)	ζ[c]	$k_{E\rightarrow Z}$[d] ($\times 10^{-6}$ s^{-1})	K_{eq}[d]
$\mathbf{3}^{E}_{Si}$ (0.27)	0.71	80	4.70	0.088	2.00 (6.30)	0.48 (−0.32)
$\mathbf{3}^{E}_{Si}$ (0.27)	0.82	100	4.31	0.130	3.35 (6.52)	0.50 (−0.30)
$\mathbf{3}^{E}_{Si}$ (0.27)	0.68	120	5.49	0.222	5.08 (6.71)	0.71 (−0.15)
$\mathbf{3}^{E}_{Si}$ (0.22)	0.67	140	5.88	0.417	12.03 (7.08)	0.65 (−0.19)

substrate	B (Torr)	T (°C)	τ[b] ($\times 10^8$ s)	ϵ[c]	$k_{Z\rightarrow E}$[d] ($\times 10^{-6}$ s^{-1})	K_{eq}[d]
$\mathbf{3}^{Z}_{Si}$ (0.29)	0.71	80	4.70	0.042	0.96 (5.98)	0.48 (−0.32)
$\mathbf{3}^{Z}_{Si}$ (0.28)	0.82	90	4.31	0.065	1.68 (6.23)	0.50 (−0.30)
$\mathbf{3}^{Z}_{Si}$ (0.28)	0.68	100	5.49	0.158	3.62 (6.56)	0.71 (−0.15)
$\mathbf{3}^{Z}_{Si}$ (0.22)	0.67	120	5.88	0.272	7.85 (6.89)	0.65 (−0.19)

[a] CH_3Cl, 750 Torr; $H_2{}^{18}O$, 3 Torr; O_2, 6 Torr; radiation dose, 2×10^4 Gy (dose rate, 1×10^4 Gy h^{-1}). [b] Reaction time, τ, calculated from the reciprocal of the first-order collision constant between intermediates $\mathbf{II}^{E}_{Si}$ and $\mathbf{II}^{Z}_{Si}$ and B. [c] $\zeta = [\mathbf{2}^{Z}_{Si}]/([\mathbf{2}^{E}_{Si}] + [\mathbf{2}^{Z}_{Si}])$; $\epsilon = [\mathbf{2}^{E}_{Si}]/([\mathbf{2}^{E}_{Si}] + [\mathbf{2}^{Z}_{Si}])$. Each value is the average of several determinations, with an uncertainty level of ∼5%. [d] See text; log k and log K_{eq} in parentheses.

Linear correlations are observed between the logarithm of $k_{E\rightarrow Z}$ and $k_{Z\rightarrow E}$ and the inverse of temperature (Figure 2, X = F; Figure 3, X = Si(CH$_3$)$_3$). Table 6 reports the relevant Arrhenius equations and activation parameters, as calculated from the transition-state theory equation. According to these values, intermediate $\mathbf{II}^{E}_F$ is more stable than epimer $\mathbf{II}^{Z}_F$ by 1.0 ± 0.7 kcal mol^{-1}. In contrast, intermediate $\mathbf{II}^{E}_{Si}$ is less stable than epimer $\mathbf{II}^{Z}_{Si}$ by 1.9 ± 1.3 kcal mol^{-1}.

Considering the uncertainties associated in the experimental measurements and theoretical calculations (±2 kcal mol^{-1}), the experimental $\mathbf{II}^{Z}_F < \mathbf{II}^{E}_F$ and $\mathbf{II}^{Z}_{Si} > \mathbf{II}^{E}_{Si}$ stability trends can be taken as coinciding with the B3LYP/6-31G* calculated ones

(17) The collision constant k_b between $\mathbf{II}^{Z}_X$ (or $\mathbf{II}^{E}_X$) and $(C_2H_5)_3N$ is calculated according to: Su, T.; Chesnavitch, W. J. *J. Chem. Phys.* 1982, *76*, 5183.

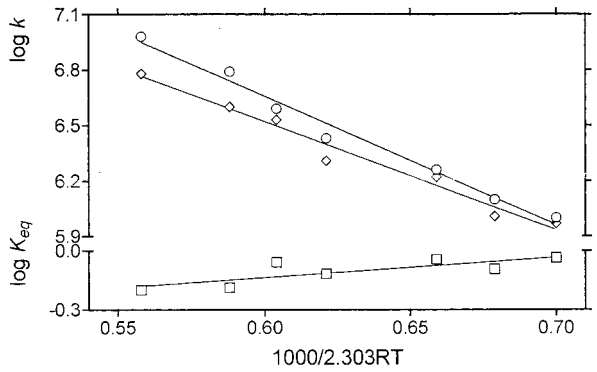

Figure 2. Temperature dependence of the $k_{E\rightarrow Z}$ (circles) and $k_{Z\rightarrow E}$ (diamonds) rates and of the relevant $K_{eq} = k_{Z\rightarrow E}/k_{E\rightarrow Z}$ (squares) concerning the gas-phase $\mathbf{II}^{Z}_{F} \rightleftarrows \mathbf{II}^{E}_{F}$ epimerization.

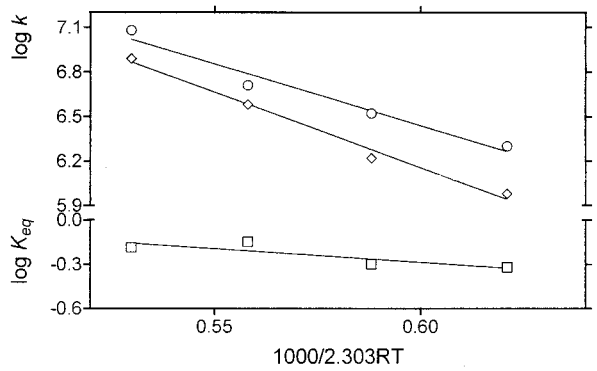

Figure 3. Temperature dependence of the $k_{E\rightarrow Z}$ (circles) and $k_{Z\rightarrow E}$ (diamonds) rates and of the relevant $K_{eq} = k_{Z\rightarrow E}/k_{E\rightarrow Z}$ (squares) concerning the gas-phase $\mathbf{II}^{Z}_{Si} \rightleftarrows \mathbf{II}^{E}_{Si}$ epimerization.

($\Delta H°(\mathbf{II}^{E}_{F}) - \Delta H°(\mathbf{II}^{Z}_{F}) = 0.81$ kcal mol^{-1}; $\Delta H°(\mathbf{II}^{E}_{Si}) - \Delta H°(\mathbf{II}^{Z}_{Si}) = -0.03$ kcal mol^{-1}) (Table 1).

Knowledge of the $\mathbf{II}^{Z}_{X} \rightleftarrows \mathbf{II}^{E}_{X}$ epimerization extent during the ion lifetime τ allows k_{syn}/k_{anti} of Scheme 1 to be expressed as follows:

$$\frac{k_{syn}}{k_{anti}} = \frac{[\mathbf{2}^{Z}_{X}] - \zeta}{[\mathbf{2}^{E}_{X}] - \epsilon} \qquad \text{(eq XIX of Appendix)}$$

with the $[\mathbf{2}^{Z}_{X}]$ and $[\mathbf{2}^{E}_{X}]$ values as listed in Tables 2 and 3 and the ζ and ϵ terms, as recalculated at $t = \tau$ of Tables 2 and 3 using eqs VIII and VII of the Appendix, respectively. The k_{syn}/k_{anti} ratios are reported in Figure 4 as a function of T^{-1}. Table 7 reports the relevant Arrhenius equations and activation parameters, as calculated from the transition-state theory equation. According to these values, the 298 K enthalpy and free energy profiles of the gas-phase *extracomplex* addition of CH_3OH to $\mathbf{I}_F$ and $\mathbf{I}_{Si}$ (path i of Scheme 1) can be depicted as in Figure 5a and b, respectively. The 298 K enthalpy and free energy profiles of the gas-phase *intracomplex* addition of CH_3OH to $\mathbf{I}_F$ and $\mathbf{I}_{Si}$ (path ii of Scheme 1) are reported in Figure 6a and b, respectively.

The enthalpy and free energy level of the relevant complexes $\mathbf{III}_X$ remain undefined. However, the poor dependence of the absolute yields of the ethereal products $\mathbf{2}^{E}_{X}$ and $\mathbf{2}^{Z}_{X}$ upon temperature (Tables 2 and 3) points to the enthalpy and free energy of the corresponding $\mathbf{III}_X$ as falling rather close to those of the two relevant transition structures $TS_X{}^{anti}$ and $TS_X{}^{syn}$.

The results summarized in Figures 5 and 6 indicate that (1) the gas-phase addition of CH_3OH to ion $\mathbf{I}_F$ is characterized by significant adverse activation entropies; (2) the same reaction on ion $\mathbf{I}_{Si}$ involves less significant activation entropies; (3) anti attack of CH_3OH on both ions $\mathbf{I}_F$ and $\mathbf{I}_{Si}$ is enthalpically favored over the competing syn addition irrespective of whether it proceeds through the extracomplex i or the intracomplex pathway ii; (4) the preferred syn diastereoselectivity, observed with ion $\mathbf{I}_F$ at $T \geq 20$ °C (Table 2), is determined by the large adverse *entropic* factors and not by the enthalpy terms; (5) contrariwise, the anti > syn selectivity, measured with ion $\mathbf{I}_{Si}$ at $T \geq 20$ °C (Table 3), is essentially governed by the relevant activation enthalpies; (6) adverse entropy factors are more important in the intracomplex anti attack of CH_3OH on $\mathbf{I}_{Si}$ (Figure 6b) than in the extracomplex one (Figure 5b).

Discussion

Transition Structures. Some information about the transition structures $TS_X{}^{anti}$ and $TS_X{}^{syn}$ of Figures 5 and 6 may be inferred from the comparison between the B3LYP/6-31G* C−O bond dissociation energies of oxonium ions $\mathbf{II}^{Z}_{X}$ and $\mathbf{II}^{E}_{X}$ (Table 1) and the experimental activation enthalpies of the gas-phase $\mathbf{II}^{Z}_{X} \rightleftarrows \mathbf{II}^{E}_{X}$ epimerization (Table 6). It is noted that the experimental $\Delta H^{‡}$ values of the $\mathbf{II}^{Z}_{Si} \rightleftarrows \mathbf{II}^{E}_{Si}$ epimerization (Table 6) are comparable to the theoretical C−O bond dissociation energies of the interconverting oxonium ions (Table 1). This indicates that the $\mathbf{II}^{Z}_{Si} \rightleftarrows \mathbf{II}^{E}_{Si}$ epimerization proceeds through loose transition structures $TS_{Si}{}^{anti}$ and $TS_{Si}{}^{syn}$, characterized by the almost complete C−O bond cleavage and by no intense interactions of the moving methanol with the $\mathbf{I}_{Si}$ moiety. However, comparison of Figures 5b and 6b shows that, while the extracomplex (i) and the intracomplex syn addition (ii) in $\mathbf{III}_{Si}$ exhibit equally large activation barriers, the enthalpy barrier involved in the intracomplex anti addition (ii) in $\mathbf{III}_{Si}$ (Figure 6b) is 1.6 kcal mol^{-1} lower than that governing the corresponding extracomplex reaction i (Figure 5b). This suggests that, while the syn addition in $\mathbf{III}_{Si}$ proceeds through a single loose transition structure $TS_{Si}{}^{syn}$, the corresponding anti addition in $\mathbf{III}_{Si}$ may involve two different $TS_{Si}{}^{anti}$ transition structures with very similar activation free energies in the temperature range investigated. One is characterized by a loose structure similar to that involved in the competing syn addition (Figure 5b). The lower enthalpy value associated with $TS_{Si}{}^{anti}$ of Figure 6b is instead consistent with a much tighter structure. The fact that the latter $TS_{Si}{}^{anti}$ is involved in the intracomplex addition (ii), where the incipient $CH_3{}^{18}OH$ nucleophile *is necessarily proton bonded* to the CH_3 hydrogens of $\mathbf{I}_{Si}$, provides strong support in favor of a structure where the methanol molecule is specifically coordinated between the C2 center and the adjacent acidic CH_3 hydrogens of the $\mathbf{I}_{Si}$ moiety.

The experimental $\Delta H^{‡}$ values of the $\mathbf{II}^{Z}_{F} \rightleftarrows \mathbf{II}^{E}_{F}$ interconversion (Table 6) amounts to only half of the theoretical C−O bond dissociation energies of the involved cations (Table 1). This points to the $\mathbf{II}^{Z}_{F} \rightleftarrows \mathbf{II}^{E}_{F}$ epimerization as proceeding through transition structures $TS_F{}^{anti}$ and $TS_F{}^{syn}$ characterized by a limited C−O bond elongation. The coincidence of the activation parameters of the extracomplex addition i in $\mathbf{III}_F$ (Figure 5a) with those of the intracomplex reaction ii (Figure 6a) indicates that both syn and anti attacks involve tight transition structures. This hypothesis finds further support in the large adverse[18] activation entropies associated in their formation (Figures 5a and 6a). The same correspondence is observed with regard to the tight, strongly coordinated transition

(18) In the frame of transition structures resembling the corresponding $\mathbf{III}_X$ adducts, the adverse activation entropies associated with their formation can be accounted for inter alia by the large structural distortion of the $\mathbf{I}_X$ moiety which is a symptom of a diffuse, pronounced torsional freezing.

Table 6. Arrhenius Parameters for the Gas-Phase Epimerization of $\mathbf{II}^{E}_{X}$ and $\mathbf{II}^{Z}_{X}$

epimerization reaction	Arrhenius equation[a]	corr coeff r^2	$\Delta H^{\ddagger}$ (kcal mol^{-1})	$\Delta S^{\ddagger}$ (cal mol^{-1} K^{-1})
$\mathbf{II}^{E}_{F} \rightarrow \mathbf{II}^{Z}_{F}$	$\log k_{E\rightarrow Z} = (10.8 \pm 0.3) - (6.9 \pm 0.4)x$	0.983	6.2 ± 0.5	-11.5 ± 1.3
$\mathbf{II}^{Z}_{F} \rightarrow \mathbf{II}^{E}_{F}$	$\log k_{Z\rightarrow E} = (10.0 \pm 0.3) - (5.9 \pm 0.4)x$	0.974	5.2 ± 0.5	-14.7 ± 2.1
$\mathbf{II}^{E}_{Si} \rightarrow \mathbf{II}^{Z}_{Si}$	$\log k_{E\rightarrow Z} = (11.4 \pm 0.6) - (8.3 \pm 1.1)x$	0.966	7.5 ± 1.1	-8.8 ± 4.2
$\mathbf{II}^{Z}_{Si} \rightarrow \mathbf{II}^{E}_{Si}$	$\log k_{Z\rightarrow E} = (12.2 \pm 0.4) - (10.1 \pm 0.8)x$	0.988	9.4 ± 0.7	-4.8 ± 2.9

[a] $x = 1000/2.303RT$.

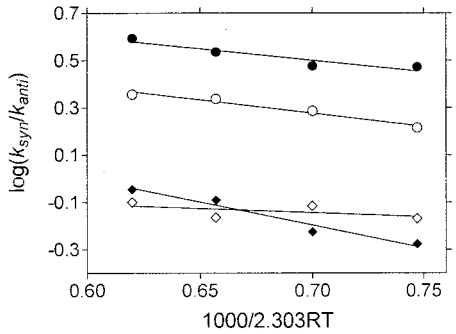

Figure 4. Temperature dependence of the k_{syn}/k_{anti} ratios concerning the gas-phase extracomplex (open symbols) and intracomplex (solid symbols) addition of $CH_3{}^{18}OH$ to $\mathbf{I}_F$ (circles) and $\mathbf{I}_{Si}$ (diamonds).

structure $TS_{Si}{}^{anti}$ involved in the intracomplex $\mathbf{II}^{E}_{Si} \rightarrow \mathbf{III}_{Si}$ process (Figure 6b). By the same token, the loose transition structures $TS_{Si}{}^{anti}$, involved in the extracomplex $\mathbf{II}^{E}_{Si} \rightarrow \mathbf{III}_{Si}$ process (Figure 5b), and $TS_{Si}{}^{syn}$ are consistent with the comparatively limited activation entropies accompanying their formation (Figures 5b and 6b).

Origin of the Diastereofacial Selectivity. Irrespective of the specific reaction pathway, whether (i) or (ii) of Scheme 1, the gas-phase anti attack of CH_3OH to ions $\mathbf{I}_F$ and $\mathbf{I}_{Si}$ involves activation enthalpies lower than those of the corresponding syn reaction (Figures 5 and 6). These findings may be rationalized in terms of the Leffler−Hammond postulate[19] by assuming that the difference in the activation barriers of the anti and syn addition of CH_3OH to $\mathbf{I}_X$ is directly proportional to the stability difference of the corresponding addition products, i.e., $\mathbf{II}^{E}_{X}$ and $\mathbf{II}^{Z}_{X}$, respectively. In other words, the substituent effect on the activation barriers of the gas-phase anti and syn addition of CH_3OH to $\mathbf{I}_X$ is somewhat expressed by changes in the relative stability of the reaction products.

The observed predominance of syn attack on $\mathbf{I}_F$ at $T \geq 20$ °C (Table 2) is due to *large adverse entropic factors reversing the enthalpic diastereoselectivity* (Figures 5a and 6a). The different adverse activation entropy associated with the competing syn and anti additions is ascribed to the different physical space available to the CH_3OH nucleophile in its approach to the *zu* and *en* faces of the distorted ion $\mathbf{I}_F$ (Figure 1a).

As pointed out in the previous section, the gas-phase addition of CH_3OH on $\mathbf{I}_{Si}$ involves more limited entropic factors. Their effect is insufficient to reverse the enthalpic diastereoselectivity (Figures 5b and 6b), thereby, the prevalence of anti attack of CH_3OH on $\mathbf{I}_{Si}$ (Table 3).

Comparison with Related Solution Data. In their seminal work,[2,3] le Noble at al. reported on the diastereoselectivity of chloride ion attack on 2-methyl-5-F-2-adamantyl cations $\mathbf{I}_F$, generated in CH_2Cl_2 by reaction of gaseous HCl with (*E*)- and (*Z*)-2-methyl-5-fluoro-2-hydroxyadamantane ($\mathbf{3}^{E}_{F}$ and $\mathbf{3}^{Z}_{F}$, respectively). The dominant product from this reaction is the *Z* chloride which exceeds the *E* chloride by a factor of 3 to 1 or more. Le Noble et al. explained the origin of this stereoselectivity in terms of the differential hyperconjugative stabilization of two rapidly equilibrating σ-delocalized 2-methyl-5-F-2-adamantyl cations. The possibility that hyperconjugative stabilization in these ions is facilitated by partial pyramidalization of the cationic C2 center was advanced after comprehensive ^{13}C NMR[20,21] and ab initio[22,23] studies on related ionic intermediates. Accordingly, diastereoselectivity in 5-substituted-2-adamantyl cations is ascribed to different hyperconjugative effects of the substituent at C5 on the relative stability of rapidly equilibrating pyramidalized syn and anti ions prior to nucleophilic attack.[4]

This picture is not corroborated by the present B3LYP/6-31G* calculations. Accordingly, the 2-methyl-5-F-2-adamantyl cation $\mathbf{I}_F$ presents a single syn pyramidalized structure (Figure 1a), whereas the 2-methyl-5-Si$(CH_3)_3$-2-adamantyl cation $\mathbf{I}_{Si}$ exhibits a single anti pyramidalized geometry (Figure 1b). Occurrence of a single structure precludes the intrinsic diastereoselectivity of these cations being influenced by an equilibrium population of the two syn/anti invertomers. Rather, the present kinetic results demonstrated that it is mainly determined by the relative stability of their addition products with methanol and that entropic factors may play a major role. In this connection, it should be noted that the gas-phase diastereoselectivity of ions $\mathbf{I}_F$ and $\mathbf{I}_{Si}$ toward methanol, expressed by the relevant 20 °C k_{syn}/k_{anti} ratios., i.e., 1.6−3.0 ($\mathbf{I}_F$) and 0.5−0.7 ($\mathbf{I}_{Si}$) (Tables 2 and 3 using eq XIX), is much less pronounced than that of the same ions toward the chloride anion in solution, i.e., 9.0 ($\mathbf{I}_F$) and 0.5 ($\mathbf{I}_{Si}$) in CH_2Cl_2 (dielectric constant, 8.9) and >50 ($\mathbf{I}_F$) and 1.0 ($\mathbf{I}_{Si}$) in CH_3NO_2 (dielectric constant, 37.5).[4,6] This diverging behavior cannot be satisfactory explained in terms of equilibrating syn/anti $\mathbf{I}_F$ and $\mathbf{I}_{Si}$ structures, allowed by specific solvent effects in solution. In fact, the conceivable coexistence in solution of any anti pyramidalized form with the more stable syn 2-methyl-5-F-2-adamantyl structure would lead to a diastereoselectivity in solution *lower* and not greater than that measured in the gas phase. The same argument applies for the conceivable coexistence of any syn pyramidalized structure with the more stable anti form of the solvated 2-methyl-5-Si$(CH_3)_3$-2-adamantyl cation. Hence, the higher diastereoselectivity monitored in solution may find a plausible rationale only in the differential solvation of the two faces of a pyramidalized 2-methyl-5-substituted-2-adamantyl cation. Indeed, differential solvation may modify the cage viscosity contribution to the addition activation barrier as well as the associated activation entropy. The importance of differential face solvation is strictly related to the factors stabilizing $\mathbf{I}_X$ in solution, i.e., solvation and/or hyperconjugation, and their relative contribution. This

(19) (a) Leffler, J. E. *Science* **1953**, *117*, 340. (b) Hammond, G. S. *J. Am. Chem. Soc.* **1955**, *77*, 334.

(20) Finne, E. S.; Gunn, J. R.; Sorensen, T. S. *J. Am. Chem. Soc.* **1987**, *109*, 7816.

(21) Buffam, D. J.; Sorensen, T. S.; Withworth, S. M. *Can. J. Chem.* **1990**, *68*, 1889.

(22) Dutler, R.; Rauk, A.; Sorensen, T. S.; Withworth, S. M. *J. Am. Chem. Soc.* **1989**, *111*, 9024.

(23) Rauk, A.; Sorensen, T. S.; Maerker, C.; Carneiro, J. W. de M.; Sieber, S.; Schleyer, P. v. R. *J. Am. Chem. Soc.* **1996**, *118*, 3761.

Table 7. Differential Arrhenius Parameters for the Formation of $\mathbf{II}^{E}_{X}$ and $\mathbf{II}^{Z}_{X}$ from the Gas-Phase Attack of $CH_3{}^{18}OH$ on $\mathbf{I}_X$

reaction path	Arrhenius equation[a]	corr coeff r^2	$\Delta\Delta H^{\ddagger}$ (kcal mol^{-1})	$\Delta\Delta S^{\ddagger}$ (cal mol^{-1} K^{-1})
	X = F			
i	$\log(k_{syn}/k_{anti}) = (1.1 \pm 0.1) - (1.1 \pm 0.2)x$	0.965	1.1 ± 0.1	$+4.9 \pm 0.6$
ii	$\log(k_{syn}/k_{anti}) = (1.2 \pm 0.2) - (1.0 \pm 0.2)x$	0.885	1.0 ± 0.2	$+5.4 \pm 1.0$
	X = Si(CH$_3$)$_3$			
i	$\log(k_{syn}/k_{anti}) = (0.1 \pm 0.2) - (0.4 \pm 0.4)x$	0.328	0.4 ± 0.4	$+0.5 \pm 1.7$
ii	$\log(k_{syn}/k_{anti}) = (1.2 \pm 0.2) - (2.0 \pm 0.3)x$	0.959	2.0 ± 0.3	$+5.4 \pm 1.2$

[a] $x = 1000/2.303RT$.

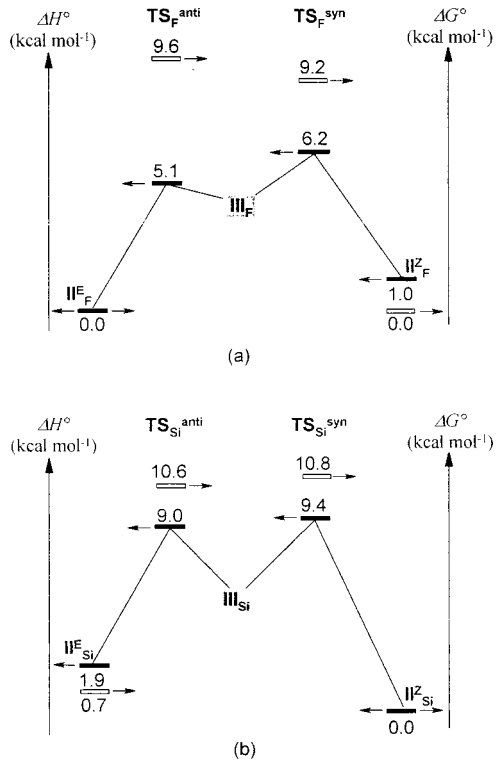

Figure 5. The 298 K enthalpy (solid bars) and free energy (open bars) profiles of the gas-phase extracomplex addition of $CH_3{}^{18}OH$ to $\mathbf{I}_F$ (a) and $\mathbf{I}_{Si}$ (b) (path i of Scheme 1).

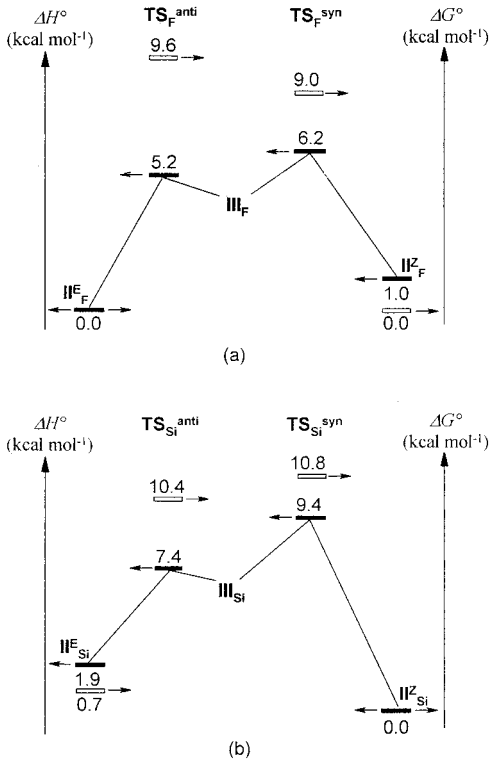

Figure 6. The 298 K enthalpy (solid bars) and free energy (open bars) profiles of the gas-phase intracomplex addition of $CH_3{}^{18}OH$ to $\mathbf{I}_F$ (a) and $\mathbf{I}_{Si}$ (b) (path ii of Scheme 1).

may account for the pronounced substituent and solvent effects on the $\mathbf{I}_X$ diastereoselectivity observed in solution.

Conclusions. The present results provide some insights into the intrinsic factors governing diastereofacial selectivity of several representative 2-methyl-5-X-2-adamantyl cations, i.e., $\mathbf{I}_F$ (X = F) and $\mathbf{I}_{Si}$ (X = Si(CH$_3$)$_3$), toward methanol. Theoretical calculations point to stable pyramidalized syn $\mathbf{I}_F$ and anti $\mathbf{I}_{Si}$ structures. The gas-phase addition of methanol to $\mathbf{I}_F$ proceeds through tight transition structures, while the same reaction on $\mathbf{I}_{Si}$ involves much looser transition structures. Anti attack of methanol on $\mathbf{I}_F$ and $\mathbf{I}_{Si}$ is enthalpically favored over the competing syn addition. The relevant enthalpy barriers reflect the relative stability of the corresponding addition products. However, large adverse activation entropies are associated with the tight transition structures for $\mathbf{I}_F$ to make the anti activation free energy higher than that of the syn structure in the 20−80 °C temperature range. Entropy factors are much less pronounced in the loose transition structures for $\mathbf{I}_{Si}$. Therefore, anti attack of methanol on $\mathbf{I}_{Si}$ is invariably preferred in the same temperature range. Comparison of the gas-phase $\mathbf{I}_F$ and $\mathbf{I}_{Si}$ diastereoselectivity with the more pronounced ones observed in solution is explained in terms of the differential solvation of the two faces of the 2-methyl-5-X-2-adamantyl pyramidalized ions in the condensed phase.

Acknowledgment. This work was supported by the Italian Ministero della Università e della Ricerca Scientifica e Tecnologica (MURST) and the Italian Consiglio Nazionale delle Ricerche (CNR) of Italy, the Australian Research Council, and the Canadian Natural Sciences and Engineering Research Council (NSERC)

Supporting Information Available: B3LYP/6-31G* data for the optimized structures $\mathbf{I}_F$ and $\mathbf{I}_{Si}$; energy profiles for fixed distortions of the C2−C6−C11 angle in the same ions. This material is available free of charge via the Internet at http://pubs.acs.org.

Appendix

In the $\mathbf{II}^{Z}_{X} \rightleftarrows \mathbf{II}^{E}_{X}$ epimerization, if initially only $\mathbf{II}^{Z}_{X}$ is present with a yield factor $[\mathbf{II}^{Z}_{X}] = 1$ and its fraction ϵ has reacted at time t, then the differential eq I

$$d[\mathbf{II}^{E}_{X}]/dt = k_{Z\rightarrow E}[\mathbf{II}^{Z}_{X}] - k_{E\rightarrow Z}[\mathbf{II}^{E}_{X}] \qquad (I)$$

may be rewritten with $[\mathbf{II}^{Z}_{X}] = 1 - \epsilon$ and $[\mathbf{II}^{E}_{X}] = \epsilon$:

$$d\epsilon/dt = k_{Z\rightarrow E}(1 - \epsilon) - k_{E\rightarrow Z}\epsilon \qquad (II)$$

According to the principle of microscopic reversibility, at the equilibrium, $t = \infty$, $\epsilon = \epsilon_{eq}$ and

$$d\epsilon/dt = 0$$

$$d\epsilon/dt = 0 = k_{Z\rightarrow E}(1 - \epsilon_{eq}) - k_{E\rightarrow Z}\epsilon_{eq} \quad \text{(III)}$$

Then

$$k_{Z\rightarrow E}(1 - \epsilon_{eq}) = k_{E\rightarrow Z}\epsilon_{eq}; \quad k_{E\rightarrow Z} = (k_{Z\rightarrow E}(1 - \epsilon_{eq}))/\epsilon_{eq} \quad \text{(IV)}$$

Introducing eq IV into eq II

$$\frac{d\epsilon}{dt} = k_{Z\rightarrow E}(1 - \epsilon) - \frac{k_{Z\rightarrow E}(1 - \epsilon_{eq})\epsilon}{\epsilon_{eq}} = \frac{k_{Z\rightarrow E}(\epsilon_{eq} - \epsilon)}{\epsilon_{eq}} \quad \text{(V)}$$

By integrating eq V and considering that $\epsilon = 0$ at $t = 0$

$$\ln\left\{\frac{\epsilon_{eq}}{(\epsilon_{eq} - \epsilon)}\right\} = \frac{k_{Z\rightarrow E}t}{\epsilon_{eq}} \quad \text{(VI)}$$

Then

$$k_{Z\rightarrow E} = \frac{\epsilon_{eq}}{t}\ln\left\{\frac{\epsilon_{eq}}{(\epsilon_{eq} - \epsilon)}\right\} \quad \text{(VII)}$$

A similar expression may be derived for the reverse reaction:

$$k_{E\rightarrow Z} = \frac{\zeta_{eq}}{t}\ln\left\{\frac{\zeta_{eq}}{(\zeta_{eq} - \zeta)}\right\} \quad \text{(VIII)}$$

if initially only $\mathbf{II}^{E}_{X}$ is present with a yield factor $[\mathbf{II}^{E}_{X}] = 1$ and its fraction ζ has reacted at time t. By definition (eq IV), the equilibrium constant, K_{eq}, is given

$$K_{eq} = \frac{k_{Z\rightarrow E}}{k_{E\rightarrow Z}} = \frac{\epsilon_{eq}}{1 - \epsilon_{eq}} = \frac{1 - \zeta_{eq}}{\zeta_{eq}} \quad \text{(IX)}$$

Then

$$\epsilon_{eq} = \frac{K_{eq}}{1 + K_{eq}} = \frac{k_{Z\rightarrow E}}{k_{Z\rightarrow E} + k_{E\rightarrow Z}} \quad \text{(X)}$$

and

$$\zeta_{eq} = \frac{1}{1 + K_{eq}} = \frac{k_{E\rightarrow Z}}{k_{Z\rightarrow E} + k_{E\rightarrow Z}} \quad \text{(XI)}$$

Equation VI may be rewritten:

$$k_{Z\rightarrow E}t/\epsilon_{eq} = \ln \epsilon_{eq} - \ln(\epsilon_{eq} - \epsilon) \quad \text{(XII)}$$

Analogously, for the reverse reaction

$$k_{E\rightarrow Z}t/\zeta_{eq} = \ln \zeta_{eq} - \ln(\zeta_{eq} - \zeta) \quad \text{(XIII)}$$

Introducing eq X into eq XII

$$t(k_{Z\rightarrow E} + k_{E\rightarrow Z}) = \ln\left\{\frac{k_{Z\rightarrow E}}{k_{Z\rightarrow E} + k_{E\rightarrow Z}}\right\} - \ln\left\{\frac{k_{Z\rightarrow E}}{k_{Z\rightarrow E} + k_{E\rightarrow Z}} - \epsilon\right\} \quad \text{(XIV)}$$

In the same way, introducing eq XI into eq XIII

$$t(k_{Z\rightarrow E} + k_{E\rightarrow Z}) = \ln\left\{\frac{k_{E\rightarrow Z}}{k_{Z\rightarrow E} + k_{E\rightarrow Z}}\right\} - \ln\left\{\frac{k_{E\rightarrow Z}}{k_{Z\rightarrow E} + k_{E\rightarrow Z}} - \zeta\right\} \quad \text{(XV)}$$

Combining eqs XIV and XV at the same reaction time t and under identical conditions

$$\epsilon/k_{Z\rightarrow E} = \zeta/k_{E\rightarrow Z} \quad \text{(XVI)}$$

and then

$$K_{eq} = \epsilon/\zeta \quad \text{(XVII)}$$

The measured $[\mathbf{2}^{Z}_{X}]$ and $[\mathbf{2}^{E}_{X}]$ yield factors of Tables 2 and 3 may be expressed

$$[\mathbf{2}^{Z}_{X}] = [\mathbf{2}^{Z}_{X}]_{true} - \epsilon[\mathbf{2}^{Z}_{X}]_{true} + \zeta[\mathbf{2}^{E}_{X}]_{true} \quad \text{and}$$

$$[\mathbf{2}^{E}_{X}] = [\mathbf{2}^{E}_{X}]_{true} - \zeta[\mathbf{2}^{E}_{X}]_{true} + \epsilon[\mathbf{2}^{Z}_{X}]_{true} \quad \text{(XVIII)}$$

Recalling that $[\mathbf{2}^{Z}_{X}]_{true} + [\mathbf{2}^{E}_{X}]_{true} = 1$

$$[\mathbf{2}^{Z}_{X}]_{true} = \frac{[\mathbf{2}^{Z}_{X}] - \zeta}{1 - \epsilon - \zeta} \quad \text{and} \quad [\mathbf{2}^{E}_{X}]_{true} = \frac{[\mathbf{2}^{E}_{X}] - \epsilon}{1 - \epsilon - \zeta} \quad \text{(XIX)}$$

JA010352L